Locating a microseismic event using deconvolution

Johannes Douma[1], Roel Snieder[1], Ashley Fish[1], and Paul Sava[1]
[1] *Center for Wave Phenomena, Colorado School of Mines, Golden, Colorado 80401*

ABSTRACT
We demonstrate a technique to enhance the ability of imaging the location of a microseismic event by improving both spatial and temporal focusing. The technique improves locating a microseismic event in a velocity model for which the interface boundaries are approximate but where it has the correct mean slowness. Our method designs a signal to be rebroadcasted from the receivers, using only the waves recorded at each receiver, such that the wave field has an optimal temporal focus at the source location. Additionally, this procedure leads to an improved spatial focus of the wave field. The numerical test shown include additive noise. This proposed technique only involves a simple preprocessing step to the recorded data and its cost is hence negligible compared to the total cost of microseismic imaging.

Key words: Microseismic, Time reversal, Deconvolution

1 INTRODUCTION

Microseismic events occur naturally or as a result of production or hydraulic stimulation (Duncan, 2005; Kendall et al., 2011). Clusters of microseismic events delineate faults and the formation of fractures and can indicate new or reactivating regions of failure. As hydraulic fracturing is becoming increasingly widespread, operators are aiming to monitor the induced events in order to characterize a reservoir. This has lead to a need from the industry to develop more accurate ways of locating and monitoring microseismic events (Foulger and Julian, 2012).

A standard processing method is based on picking arrival times of P and S waves. This process is, however, difficult when significant noise is present in the data and thus can require extensive user interaction (Bancroft et al., 2010; Bose et al., 2009; Hayles et al., 2011; Kummerow, 2010; Song et al., 2010). An alternative approach to locate events is by imaging the time reversed signal to focus microseismic signal at the source position (Artman et al., 2010; Lu and Willis, 2008; Lu, 2008; Steiner et al., 2008). The advantage of imaging the time reversed signal is that it does not require picking of arrival times, this is of particular importance for noisy data. In the imaging approach, one usually uses time reversal to focus the recorded waves at the source location in space and time (Artman et al., 2010).

If one time reverses the waves at every point in space, the wavefield will focus onto the original source location. If, however, the wavefield is sampled at only a limited number of locations, then it is not obvious that time reversal is the optimal way to focus energy on the original source. Much research has been carried out on focusing sparsely sampled wavefields (Aubry et al., 2001; Bertaix et al., 2004; Fink, 1997; Gallot et al., 2011; Jonsson et al., 2004; Larmat et al., 2010; Montaldo et al., 2004; Parvulescu, 1961; Roux and Fink, 2000; Tanter et al., 2001, 2000; Vignon et al., 2006). In this letter, we explore a simple extension to time reversal, based on deconvolution, as previously derived by Ulrich et al. (2012), to improve our imaging for locating a microseismic event. This method is a robust, though simplified, version of the inverse filter (Gallot et al., 2011; Tanter et al., 2000, 2001). It calculates a signal to be rebroadcast from the receiver such that the output at the focal location becomes an approximate delta function $\delta(t)$ and uses only the recorded signals at each receiver.

As with all imaging methods, reverse time imaging is unable to locate the microseismic event to a point location when the velocity model isn't the true velocity model or the aperture is poor; it causes the spatial image to defocus. We propagate the deconvolved waveforms through a smoothed version of the true slowness model. The local average of the slowness for this incorrect velocity model is equal to local average slowness of the true velocity model.

2 THEORY-DECONVOLUTION

Time reversal states that for a given recorded impulse response, a simple reversal in time of that signal followed by rebroadcasting the reversed signal from the receivers focuses an impulsive function $\delta(t)$ at the source location,

$$f(t) = \sum_i r_i(t) \star r_i(-t) \approx \delta(t) \tag{1}$$

where $\star$ denotes a convolution operator, $r_i(t)$ is the recorded impulse response at receiver i, and $r_i(-t)$ its time reversed counterpart. Equation (1) states that the autocorrelation of the recorded signal is ideally equal to a delta function. In practice, however, time reversal (TR) experiments are unable to recreate a true delta function focus as one or more conditions necessary to satisfy equation (1) are typically violated. For example, if attenuation is present in the medium, time reversal (TR) can not create a true delta function focus. Additionally, if the aperture is finite, TR experiments can not create a true delta function focus. Given these limitations, we introduce deconvolution to achieve a more impulsive focusing in time.

Let us assume that time reversal is not able to create a Dirac delta focus after rebroadcasting the time reversed impulse response. We aim to find a signal such that after rebroadcasting we get a temporal focus that is approximately equal to a Dirac delta function. Thus, we change equation (1) to

$$f(t) = \sum_i r_i(t) \star g_i(t) \approx \delta(t) \ , \tag{2}$$

where $f(t)$ is the back propagated signal at the source, $r_i(t)$ is the recorded impulse response at receiver i, and $g_i(t)$ is the signal that is back propagated to the source from receiver i. We determine the backpropogated signal $g_i(t)$ from the requirement that the right hand side of the equation (2) approximates a delta function as well as possible. In the frequency domain, this corresponds to the requirement,

$$\sum_i r_i(\omega) g_i(\omega) \approx 1 \ . \tag{3}$$

This condition defines the signal that optimizes the temporal focus at the source location. Equation (3), applied to each receiver states that

$$g_i(\omega) = \frac{1}{r_i(\omega)} \approx \frac{r_i^*(\omega)}{|r_i(\omega)|^2 + \epsilon}, \tag{4}$$

where $r(\omega)r^*(\omega) = |r(\omega)|^2$. We introduce a regularization parameter ϵ to stabilize the deconvolution that satisfies

$$\epsilon = \gamma \times mean(|r_i(\omega)|^2) \ . \tag{5}$$

where γ is a constant, which is sometimes referred to as the waterlevel parameter (Clayton and Wiggins, 1976), and the mean is calculated for each receiver over the frequencies for which the power spectrum differs significantly from zero. For small values of γ, the deconvolution may be sensitive to additive noise, whereas for larger values of γ the deconvolution reduces to time reversal. We choose the value of γ by maximizing the energy in a 80m by 80m region around the source. This process is similar to the time-domain procedure developed by Clayton and Wiggins (1976). We used a value of $\gamma = 0.272$ in all experiments shown. An inverse Fourier transform takes $g(\omega)$ back into the time domain. One can then directly rebroadcast $g(t)$ and does not have to apply a time reversal operation on $g(t)$.

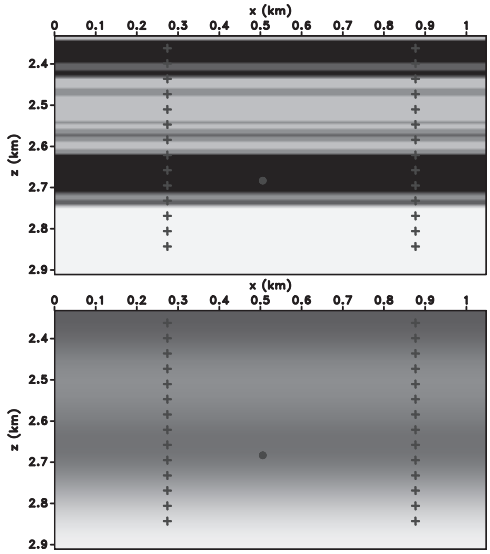

Figure 1. Velocity models of the numerical experiment. Top panel indicates the correct velocity model and represents the velocity model used to propagate the source wavefield through the medium. Bottom panel indicates the smoothed velocity model with correct mean slowness. This model is used for back propagation of the time reversed signal and optimized inverse signal. The plus symbols represent the receivers, the circular dot represents the source.

3 MICROSEISMIC EVENT LOCATING

The purpose of this study is to optimize microseismic event location using deconvolution. We use the velocity model shown in the top panel of Figure 1 to propagate the source wavefield to the receivers. The model consists of horizontally continuous layers whose velocities range from approximately 5 km/s to 6.6 km/s. In practice, one does not know the true velocity model. For this reason, we used the smoothed velocity model, shown in the bottom panel of Figure 1, for the back propagation. The velocity model is smoothed by using a two-dimensional triangle smoothing with a smoothing radius of .185 km in the z, and x direction (Fomel, 2007). This smoothed

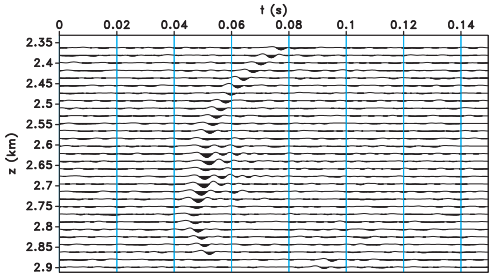

Figure 2. Wavefield excited by the source in figure 1 after propagation through the true velocity model (top panel of figure 1). Bandlimited noise is added to the data, the signal to noise ratio is .89

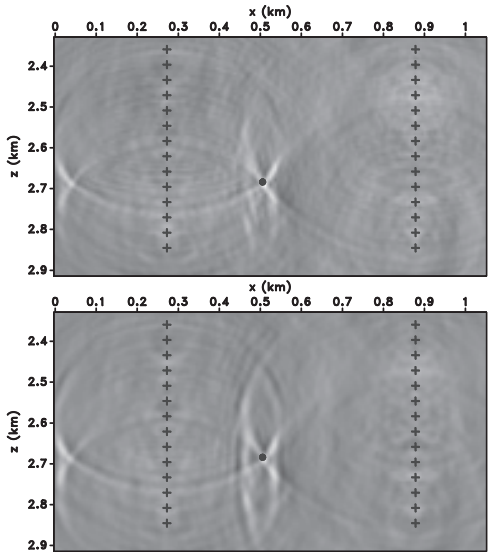

Figure 3. Wavefield $p(\mathbf{x}, t = 0)$ for deconvolution (top panel) and time reversal (bottom panel). The plus symbols represent the receivers, the circular dot represents the source. These images were created by back propagating the time reversed and inverse optimized signal through the incorrect velocity model (bottom panel of figure 1).

velocity model has the same mean slowness as the correct velocity model.

The location of the source is at $(x, z) = (0.51$ km, 2.68 km). The source wavelet is a Ricker wavelet with dominant frequency of 150 Hz. We use 56 receivers distributed over 2 vertical boreholes in our model. The x-locations of the receiver boreholes are 0.74 km and 0.88 km. The receivers range from a depth of 2.36 km to 2.86 km with a spacing of 18.5 m.

We find the focus time without knowing the triggering time. We do so by rebroadcasting our calculated inverse signal, producing an image every time step, and then calculate the energy of the spatial focus in a region around the source location until it reaches a maximum. In order to make the numerical simulation more realistic, we added noise to our recorded data at the receivers before running the time reversal or deconvolution process. Thus, both processes deal with the same noise. The additive noise only contains frequencies within the bandwidth of the data. The energy ratio of the signal to noise, defined as the ratio of the sum of the absolute values of the signal and noise squared, is equal to 0.89. The noise-contaminated data thus produced are shown in Figure 2.

As shown in Figure 3, deconvolution produces better spatial focusing than does time reversal. This allows one to find the location of the microseismic event with higher accuracy. This is possible because deconvolution suppresses the temporal sidelobes of the refocused signal and thus compresses more of the wave energy into the focus at the event time ($t = 0$). In order to compare the spatial focusing of each method, we show in figure 4(c) and (d) horizontal slices of the spatial image at the depth of the source at the time of the focus ($t = 0$). Figure 4(d) illustrates that deconvolution improves spatial focusing compared to simple time reversal (Figure 4(c)). We quantify this improved spatial focusing by computing the ratio of the energy near the focus and the total energy. Using a window centered at the source location with a width of 20 m, we calculated the energy of the focus. Dividing the energy of the focus by the total energy gives us the spatial energy ratio of the focus. Deconvolution yields a spatial energy ratio of 48% while time reversal has a spatial energy ratio of only 31%, which indicates quantitatively that deconvolution improves the spatial focus of a microseismic event.

We next consider temporal focusing. Figure 4(a) and (b) show improved temporal focusing for the deconvolution method compared to time reversal. We quantify the temporal focusing by computing the ratio of the energy near focus and the total energy. Using a window centered at $t = 0s$ with width of $.003s$, we calculated the energy of the temporal focus. Dividing this focused energy by the total energy gives us the temporal energy ratio of the focus. Deconvolution has a temporal energy ratio of 49% while time reversal has a temporal energy ratio of 40%. Thus, deconvolution improves temporal focusing.

In conclusion, deconvolution improves both temporal and spatial focusing for our model. This allows one to locate microseismic events with greater accuracy, even when the velocity model is not the true model and additive noise is present. Deconvolution improves spatial focusing even though the method we introduced is designed to improve temporal focus. It was shown by Ulrich et al. (2012) that improved temporal focusing improves spatial focusing for the spherically symmetric part of the focused wave field..

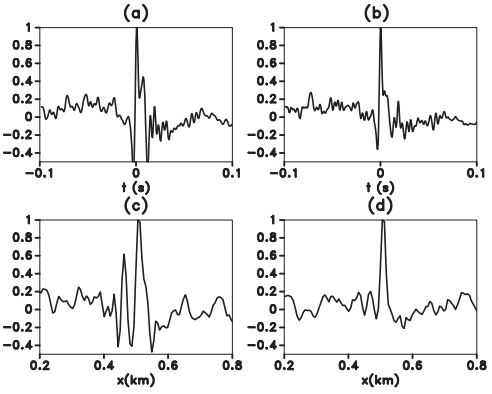

Figure 4. Temporal and spatial focused images produced by back propagating the calculated time reversed signals using time reversal and deconvolution for vertical borehole array. (a) Temporal focus at the source location obtained for time reversal, (b) Temporal focus at the source location obtained for deconvolution, (c) Horizontal cross section through the source depth at $t = 0$ obtained for time reversal, (d) Horizontal cross section through the source depth at $t = 0$ obtained for deconvolution.

4 IMPROVED TEMPORAL FOCUSING LEADS TO IMPROVED SPATIAL FOCUSING

In this section, we show that better temporal focusing implies better spatial focusing for the spherical average of the focus. We begin by first considering the wave field near its focal spot at $r = 0$ and consider the medium to be locally homogeneous in that region. The solution of the Helmholtz equation in an acoustic, homogeneous medium can be written as

$$p(r,\theta,\varphi,\omega) = \sum_{l=0}^{\infty} \sum_{m=-l}^{m=l} a_{lm} j_l(kr) Y_{lm}(\theta,\varphi) \ , \qquad (6)$$

see Table 8.2 of Arfken and Weber (2001). In this expression j_l denotes the spherical Bessel function, Y_{lm} the spherical harmonics, and $k = \omega/c$, where c is the wave speed. According to expressions (11.144) and (11.148) of Arfken and Weber (2001), $j_l(0) = 0$ for $l \geq 1$ and $j_0(0) = 1$. This means that at the focal point $r = 0$ only the terms $l = m = 0$ contribute. Using $Y_{00} = 1/\sqrt{4\pi}$ (Table 12.3 of Arfken and Weber (2001)), this means that at the focal point

$$p(r = 0,\theta,\varphi,\omega) = \frac{a_{00}}{\sqrt{4\pi}} \ . \qquad (7)$$

The properties of the wave field at the focal point thus only depend on the coefficient a_{00}. Since the $l = m = 0$ component of the spherical harmonics expansion gives the spherically symmetric component of the wave field, the properties of the wave field at the focal point can only bear a relation to the spherically symmetric component of the wave field. The properties of temporal focusing can thus be related to the spherically symmetric component of the spatial focusing only.

Because of this, we restrict ourselves to the spherically symmetric component ($l = m = 0$) of the wave field at the focal point. Using that $j_0(kr) = \sin(kr)/kr$, the spherically symmetric component of Eq. (6) is given by

$$p(r,\omega) = p_0 \ \frac{e^{-ikr} - e^{ikr}}{r} \ , \qquad (8)$$

with $p_0 = -a_{00}/(2ik\sqrt{4\pi})$. The coefficient p_0 depends on frequency. Using the Fourier convention $f(t) = \int p_0(\omega) e^{-i\omega t} d\omega$, and using that $k = \omega/c$, Eq. (8) corresponds, in the time domain, to

$$p(r,t) = \ \frac{f(t + r/c) - f(t - r/c)}{r} \ . \qquad (9)$$

In this equation, $f(t + r/c)$ denotes the wave that is incident on the focus, and $f(t - r/c)$ the outgoing wave once it has passed through the focus.The field at the focus follows by Taylor expanding $f(t \pm r/c)$ in r/c and taking the limit $r \to 0$, this gives

$$p(r = 0,t) = \frac{2}{c} f'(t) \ . \qquad (10)$$

In this expression and the following, the prime denotes the time derivative. Equation (10) states that the wave field at the focus is the time derivative of the incoming wave field and provides the temporal properties of the focus.

In order to get the spatial properties, we consider the wavefield near the focal point at time $t = 0$. Setting $t = 0$ in Eq. (9), gives

$$p(r,t = 0) = \ \frac{f(r/c) - f(-r/c)}{r} \ . \qquad (11)$$

Equation (11) states that the wave field at the time of focus is the difference between the incoming and outgoing wave and gives the spatial properties of the focus.

A improved temporal focus implies that $f'(t)$ is only nonzero for values of t close to $t = 0$. It follows from Eq. (11) that if that is the case, then $p(r, t = 0)$ is localized near $r = 0$. Note that if a constant was added to f when going from $f'(t)$ to $f(t)$, our conclusion would not change because the constant would be subtracted and cancelled out in Eq. (11).

5 CONCLUSION

We have introduced a method that improves temporal focusing of a microseismic event. The method can be beneficial for locating a microseismic event because it also improves spatial focusing compared to the standard time reversal method. We have shown how this techniques improves the locating for a microseismic event using synthetic data contaminated with additive noise.

The simplicity and robust nature of this method allows for a simple incorporation into existing reverse-time imaging methods. The cost of the deconvolution is minimal compared to running the finite difference model. Thus, it can be added as a preprocessing step without significant additional cost. Further research involves extending this method to elastic waves excited by a double couple source.

REFERENCES

Arfken, G., and H. Weber, 2001, Mathematical methods for physicists, 5th ed.: Harcourt.

Artman, B., I. Podladtchikov, and B. Witten, 2010, Source location using time-reverse imaging: Geophysical Prospecting, **58**, 861–873.

Aubry, J.-F., M. Tanter, J. Gerber, J.-L. Thomas, and M. Fink, 2001, Optimal focusing by spatio-temporal filter. II. Experiments. Application to focusing through absorbing and reverberating media: J. Acoust. Soc. Am., **110**, 48–58.

Bancroft, J. C., J. Wong, and L. Han, 2010, Sensitivity measurements for locating microseismic events: CSEG Recorder, 28–37.

Bertaix, V., J. Garson, N. Quieffin, S. Catheline, J. Derosny, and M. Fink, 2004, Time-reversal breaking of acoustic waves in a cavity: American Journal of Physics, **72**, 1308–1311.

Bose, S., H. Valero, Q. Liu, R. G. Shenoy, and A. Ounadjela, 2009, An Automatic Procedure to Detect Microseismic Events Embedded in High Noise: SEG Technical Program Expanded Abstracts, 1537–1541.

Clayton, R. W., and R. A. Wiggins, 1976, Source shape estimation and deconvolution of teleseismic body-waves: Geophys. J. Royal Astron. Soc., **47**, 151–177.

Duncan, P. M., 2005, Is there a future for passive seismic?: First Break, **23**, 111–115.

Fink, M., 1997, Time reversed acoustics: Physics Today, **50**, 34–40.

Fomel, S., 2007, Shaping regularization in geophysical-estimation problems: Geophysics, **72**, R29–R36.

Foulger, G. R., and B. R. Julian, 2012, Earthquakes and errors : Methods for industrial applications: Geophysics, **76**, WC5–WC15.

Gallot, T., S. Catheline, P. Roux, and M. Campillo, 2011, A passive inverse filter for Green's function retrieval: J. Acoust. Soc. Am., **131**, EL21–EL27.

Hayles, K., R. L. Horine, S. Checkles, J. P. Blangy, and H. Corporation, 2011, Comparison of microseismic results from the Bakken Formation processed by three different companies : Integration with surface seismic and pumping data: SEG Technical Program Expanded Abstracts, 1468–1472.

Jonsson, B. L. G., M. Gustafsson, V. H. Weston, and M. V. d. Hoop, 2004, Retrofocusing of acoustic wave fields by iterated time reversal: SIAM J. Appl. Math., **64**, 1954–1986.

Kendall, M., S. Maxwell, G. Foulger, L. Eisner, and Z. Lawrence, 2011, Special Section Microseismicity : Beyond dots in a box Introduction: Geophysics, **76**, WC1–WC33.

Kummerow, J., 2010, Using the value of the crosscorrelation coefficient to locate microseismic events: Geophysics, **75**, MA47–MA52.

Larmat, C., R. Guyer, and P. Johnson, 2010, Time-reversal methods in geophysics: Physics Today, **63**, 31–35.

Lu, R., a. T. N., and M. Willis, 2008, Locating Microseismic Events with Time Reversed Acoustics: A Synthetic Case Study: SEG Technical Program Expanded Abstracts, 1342–1346.

Lu, R., 2008, Time Reversed Acoustics and Applications to Earthquake Location and Salt Dome Flank Imaging: Massachusetts Institute of Technology. Earth Resources Laboratory.

Montaldo, G., M. Tanter, and M. Fink, 2004, Real time inverse filter focusing through iterative time reversal: J. Acoust. Soc. Am., **115**, 768–775.

Parvulescu, A., 1961, Signal detection in a multipath medium by M.E.S.S. processing: J. Acoust. Soc. Am., **33**, 1674–1674.

Roux, P., and M. Fink, 2000, Time reversal in a waveguide: study of the temporal and spatial focusing: J. Acoust. Soc. Am., **107**, 2418–2429.

Song, F., H. S. Kuleli, M. N. Toksöz, E. Ay, and H. Zhang, 2010, An improved method for hydrofracture-induced microseismic event detection and phase picking: Geophysics, **75**, A47–A52.

Steiner, B., E. H. Saenger, and S. M. Schmalholz, 2008, Time reverse modeling of low-frequency microtremors: Application to hydrocarbon reservoir localization: Geophysical Research Letters, **35**, L03307.

Tanter, M., J.-F. Aubry, J. Gerber, J.-L. Thomas, and M. Fink, 2001, Optimal focusing by spatio-temporal filter. I. Basic principles: J. Acoust. Soc. Am., **110**, 37–47.

Tanter, M., J.-L. Thomas, and M. Fink, 2000, Time reversal and the inverse filter: J. Acoust. Soc. Am., **108**, 223–234.

Ulrich, T., J. Douma, R. Snieder, and B. Anderson, 2012, Improving time reversal focusing and source reconstruction through deconvolution: J. Acoust. Soc. Am., Under Review.

Vignon, F., J.-F. Aubry, A. Saez, M. Tanter, D. Cassereau, G. Montaldo, and M. Fink, 2006, The Stokes relations linking time reversal and the inverse filter: J. Acoust. Soc. Am., **119**, 1335–1346.